Mechanisms of Oxidation of Guanine in DNA by Carbonate Radical Anion, a Decomposition Product of Nitrosoperoxycarbonate

ARTICLE *in* CHEMISTRY · MAY 2007

Impact Factor: 5.73 · DOI: 10.1002/chem.200601434 · Source: PubMed

7 AUTHORS, INCLUDING:

Young- Ae Lee
Yeungnam University
5 PUBLICATIONS **114** CITATIONS
SEE PROFILE

Seog K Kim
Yeungnam University
93 PUBLICATIONS **1,209** CITATIONS
SEE PROFILE

Peter C Dedon
Massachusetts Institute of Technology
173 PUBLICATIONS **5,376** CITATIONS
SEE PROFILE

Nicholas E Geacintov
New York University
432 PUBLICATIONS **12,045** CITATIONS
SEE PROFILE

DOI: 10.1002/chem.200601434

Mechanisms of Oxidation of Guanine in DNA by Carbonate Radical Anion, a Decomposition Product of Nitrosoperoxycarbonate

Young Ae Lee,[a] Byeong Hwa Yun,[a] Seog K. Kim,[b] Yelena Margolin,[c] Peter C. Dedon,[c] Nicholas E. Geacintov,[a] and Vladimir Shafirovich*[a]

Abstract: Peroxynitrite is produced during inflammation and combines rapidly with carbon dioxide to yield the unstable nitrosoperoxycarbonate, which decomposes (in part) to $CO_3^{\bullet-}$ and $^{\bullet}NO_2$ radicals. The $CO_3^{\bullet-}$ radicals oxidize guanine bases in DNA through a one-electron transfer reaction process that ultimately results in the formation of stable guanine oxidation products. Here we have explored these mechanisms, starting with a spectroscopic study of the kinetics of electron transfer from 20–22mer double-stranded oligonucleotides to $CO_3^{\bullet-}$ radicals, together with the effects of base sequence on the formation of the end-products in runs of one, two, or three contiguous guanines. The distributions of these alkali-labile lesions were determined by gel electrophoresis methods. The cascade of events was initiated through the use of 308 nm XeCl excimer laser pulses to generate $CO_3^{\bullet-}$ radicals by an established method based on the photodissociation of persulfate to sulfate radicals and the oxidation of bicarbonate. Although the Saito model (Saito et al., *J. Am. Chem. Soc.* **1995**, *117*, 6406–6407) predicts relative ease of one-electron oxidations in DNA, following the trend 5′-···GGG··· > 5′-···GG··· > 5′-···G···, we found that the rate constants for $CO_3^{\bullet-}$-mediated oxidation of guanines in these sequence contexts (k_5) showed only small variation within a narrow range [$(1.5–3.0)\times 10^7\,M^{-1}s^{-1}$]. In contrast, the distributions of the end-products are dependent on the base sequence context and are higher at the 5′-G in 5′-···GG··· sequences and at the first two 5′-guanines in the 5′-···GGG··· sequences. These effects are attributed to a combination of initial hole distributions among the contiguous guanines and the subsequent differences in chemical reaction yields at each guanine. The lack of dependence of k_5 on sequence context indicates that the one-electron oxidation of guanine in DNA by $CO_3^{\bullet-}$ radicals occurs by an inner-sphere mechanism.

Keywords: DNA · hole transfer · kinetics · oxidative damage · radicals

Introduction

A growing body of epidemiological evidence suggests that chronic inflammation is correlated with malignant cell transformation and thus may play a role in the etiology of some human cancers.[1–5] A central hypothesis linking inflammation and cancer is based on a mechanism that involves the formation of oxidative DNA damage under conditions of oxidative and nitrosative stress.[6–9] If not eliminated by cellular DNA repair processes, these DNA lesions can give rise to point mutations, deletions, and rearrangements that can initiate the development of cancer.[3,4] Under inflammatory conditions, neutrophils and macrophages are activated and overproduce nitric oxide and superoxide radical anions, which rapidly combine with one another to form peroxynitrite [Eq. (1)]:[10–13]

$$^{\bullet}NO + O_2^{\bullet-} \rightarrow ONOO^- \quad (1)$$

This reaction is diffusion-controlled, with a rate constant from 6.6 to $19\times10^9\,M^{-1}s^{-1}$.[14,15] In neutral aqueous solutions, peroxynitrite rapidly reacts with CO_2 ($k=3\times10^4\,M^{-1}s^{-1}$) to yield the highly unstable nitrosoperoxycarbonate anion $ONOOCO_2^-$ [Eq. (2)]:[16]

[a] Dr. Y. A. Lee, B. H. Yun, Prof. Dr. N. E. Geacintov, Prof. Dr. V. Shafirovich
Chemistry Department, 31 Washington Place
New York University, New York, NY 10003–5180 (USA)
E-mail: vs5@nyu.edu

[b] Prof. Dr. S. K. Kim
Chemistry Department, Yeongnam University
Gyongsan, Gyongbuk, 712–749 (Korea)

[c] Y. Margolin, Prof. Dr. P. C. Dedon
Biological Engineering Division
Massachusetts Institute of Technology
Cambridge, MA 02139 (USA)

$$ONOO^- + CO_2 \rightarrow ONOOCO_2^- \quad (2)$$

Homolytic dissociation of $ONOOCO_2^-$, occurring on a submicrosecond timescale,[17] produces $^{\bullet}NO_2$ and $CO_3^{\bullet-}$ radicals with a yield $f \approx 0.30$–0.35 [Eq. (3)]:[18,19]

$$ONOOCO_2^- \rightarrow f(^{\bullet}NO_2 + CO_3^{\bullet-}) + (1-f)(NO_3^- + CO_2) \quad (3)$$

Recent in vitro experiments have shown that peroxynitrite can cause DNA damage both by strand cleavage through oxidation of the deoxyribose residues[20–22] and by modification of the nucleobases.[9,23,24] The presence of carbon dioxide in reaction mixtures also containing DNA and peroxynitrite enhances nucleobase product formation while suppressing the oxidation of deoxyribose.[22] These observations are believed to indicate a shift of peroxynitrite decomposition product formation from $HO^{\bullet}$ radicals and $^{\bullet}NO_2$, in the absence of CO_2, to $CO_3^{\bullet-}$ and $^{\bullet}NO_2$ in its presence. Guanine is the base most sensitive towards oxidation, and a clear correlation has been found between sites of $ONOO^-$-induced DNA damage and $ONOO^-$-induced mutations in the *supF* gene of the pSP189 plasmid replicated in *E. coli*.[22] Consistently with the differences in chemical product distributions, significant differences were found between the mutation spectra induced by treatment of the *supF* gene with $ONOO^-$ in the absence and in the presence of CO_2.[25,26]

Of the two species produced by the decomposition of nitrosoperoxycarbonate anion, only the $CO_3^{\bullet-}$ radical can directly oxidize guanine in DNA by a one-electron transfer mechanism, and we have recently devised suitable methods for studying these reactions by laser flash photolysis techniques.[27,28] In these time-resolved experiments, $CO_3^{\bullet-}$ radicals were obtained through one-electron oxidation of HCO_3^- ions by photochemically generated sulfate radical anions ($SO_4^{\bullet-}$). The $CO_3^{\bullet-}$ radicals induce site-selective oxidation of guanine bases in DNA, a reaction that has been monitored by the rise of the characteristic transient absorption band of guanine neutral radicals (Gua(-H)$^{\bullet}$). The end-products of the latter radicals in oligonucleotides are alkali-labile lesions,[27] mostly the diastereomeric pair of spiroiminodihydantoin (Sp) lesions[28] that are formed in high yields (40–60%) by a complex series of consecutive electron-transfer reactions from guanine to the $CO_3^{\bullet-}$ radicals.[29]

Recently, base sequence effects have been explored by employment of one-electron oxidants generated by the photosensitization of metal complexes,[30,31] anthraquinones,[32,33] naphthalimides,[34] riboflavin,[35,36] benzophenone derivatives,[36,37] and 4-acylated thymidines.[38–41] Overall, the formation of hot alkali-labile lesions is most efficient in 5′-GGG, followed by 5′-GG and then by noncontiguous or isolated G (flanked by bases other than G) sequence contexts. In 5′-GG and 5′-GGG sequence contexts, product formation is also dependent on the position of a particular guanine within the GG or GGG contiguous sequence. Saito and co-workers have shown that these phenomena correlate with the calculated gas-phase ionization potentials (IPs) of guanine residues in different sequence contexts.[35,42,43] The distributions of positive charge resulting from one-electron oxidation of guanine in sequences of two or three adjacent guanines, as well as in guanines flanked by other nucleobases, have been calculated more recently.[44] We have recently shown, however, that the oxidative formation of guanine products through reactions between guanines and nitrosoperoxycarbonate in the different sequence contexts studied by Saito and co-workers yield entirely different patterns.[45]

Our long-term objectives are to reach a better understanding of these base sequence effects. Here we begin by studying the oxidation of oligonucleotides by one of the decomposition products of nitrosoperoxycarbonate: the $CO_3^{\bullet-}$ radical anion. We have used laser kinetic-spectroscopic methods to explore the characteristics of the kinetics of oxidation of guanine in G, GG, and GGG sequence contexts by $CO_3^{\bullet-}$ radicals. The ultimate products of these initial oxidation events have been revealed as strand breaks by hot piperidine or enzymatic (Fpg, formamidopyrimidine DNA *N*-glycosylase) treatment, and the resulting breaks have been quantified by high-resolution polyacrylamide gel electrophoresis methods. The mechanistic aspects of the oxidative DNA damage initiated by $CO_3^{\bullet-}$ radicals are discussed in detail.

Results and Discussion

A set of oligonucleotides (Table 1) was designed in order to explore the effects of sequence context on the initial one-electron oxidation step mediated by the carbonate radical anions and the subsequent formation of oxidized base products. The oligonucleotides were designed with systematically altered positioning of multiple guanines. All duplexes were prepared by annealing the strands with their natural complementary strands shown in Table 1.

The initial step—kinetics of one-electron oxidation of oligonucleotide duplexes by $CO_3^{\bullet-}$ radicals: A typical transient absorption spectrum of $CO_3^{\bullet-}$ radicals generated by the 308 nm laser pulses is depicted in Figure 1 (inset). The kinetics of the decay of $CO_3^{\bullet-}$ radicals can be monitored by following the decay of the absorbance signal at the 600 nm absorption maximum of the carbonate radical anions.[27,28] A typical decay curve is depicted in Figure 1 and shows that, in a solution containing the duplex **2d** (100 μM), the $CO_3^{\bullet-}$ radicals decay on a submillisecond time scale. The rate constants of DNA oxidation by $CO_3^{\bullet-}$ radicals have been derived from these decay curves by methods that have been described in detail previously.[27,28] These rate constants (k_5; defined in Table 2), have been measured with a representative set of oligonucleotide duplexes, as summarized in Table 1.

The double-stranded sequences **1d**–**7d** are 20–22 mer duplexes containing different numbers of G, A, and T residues. Interestingly, the k_5 values are all similar in value, within the rather narrow range of $(1.5$–$3.0) \times 10^7\ M^{-1}s^{-1}$. Thus, the rate

Table 1. Rate constants (k_5) for the one-electron oxidation of oligonucleotides by $CO_3^{\bullet-}$ radicals.

Designation	DNA duplex	k_5[a] [$M^{-1}s^{-1}$]
1d	5′-d(AAATT**G**TTTTTAAATT**G**TTTTT)•3′-d(TTTAACAAAAATTTAACAAAAA)	$(1.6\pm0.2)\times10^7$
2d	5′-d(AAATT**GG**TTTTAAATT**GG**TTTT)•3′-d(TTTAACCAAAATTTAACCAAAA)	$(1.5\pm0.2)\times10^7$
3d	5′-d(AAAT**GGG**TTTTAAAT**GGG**TTTT)•3′-d(TTTACCCAAAATTTACCCAAAA)	$(2.0\pm0.2)\times10^7$
4d	5′-d(AAATTT**G**TTTTTTT**G**TTTAAA)•3′-d(TTTAAACAAAAAACAAATTT)	$(2.7\pm0.3)\times10^7$
5d	5′-d(AAATTTTTT**GG**TTTTTTAAA)•3′-d(TTTAAAAAACCAAAAAATTT)	$(3.0\pm0.3)\times10^7$
6d	5′-d(AAATTT**G**TTT**G**TTT**G**TTTAAA)•3′-d(TTTAAACAAACAAACAAATTT)	$(2.5\pm0.3)\times10^7$
7d	5′-d(AAATTTTTT**GGG**TTTTTTAAA)•3′-d(TTTAAAAAACCCAAAAAATTT)	$(2.6\pm0.3)\times10^7$
8d	5′-d(TT**G**TTT**G**TTT**G**TTT**G**TTT**G**TT)•3′-d(AACAAACAAACAAACAAACAA)	n.d.
9d	5′-d(TT**G**TTT**G**TTT**GG**TTT**G**TTT**G**TT)•3′-d(AACAAACAAACCAAACAAACAA)	n.d.
10d	5′-d(TT**G**TTT**G**TTT**GGG**TTT**G**TTT**G**TT)•3′-d(AACAAACAAACCCAAACAAACAA)	n.d.
11d	5′-d(AAC**GC**G**A**ATTC**GC**GTT)•3′-d(TTGCGCTTAAGCGCAA)	$(1.9\pm0.2)\times10^7$ (Ref. [27])
dGMP	2′-deoxyguanosine 5′-monophosphate	$(6.7\pm0.7)\times10^7$ (Ref. [27])

[a] The rate constants were measured in air-equilibrated buffer solutions (pH 7.5) at (23±2)°C. The uncertainties represent standard errors for the best least-squares fits of the appropriate kinetic equations to the experimentally measured decay profiles of $CO_3^{\bullet-}$ radicals measured at 600 nm resulting from the 308 nm laser pulse excitation.

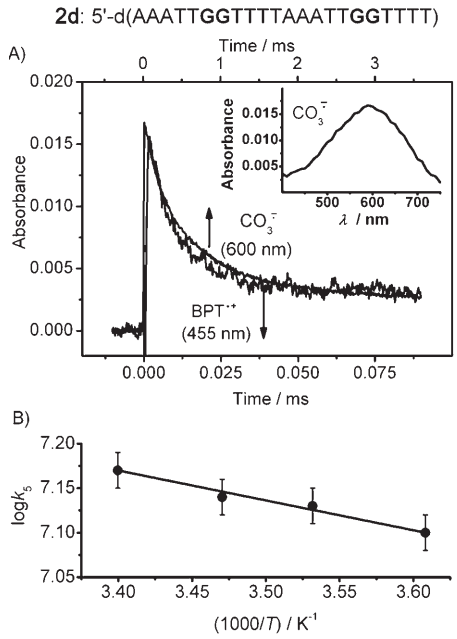

Figure 1. A) Kinetics of $CO_3^{\bullet-}$ and $BPT^{\bullet+}$ decay in the presence of an oligonucleotide duplex (**2d**, 100 μM) containing a single GG-doublet, recorded after a single-short photoexcitation pulse—an actinic 308 nm excimer laser pulse ($CO_3^{\bullet-}$) or a 355 nm Nd:Yag laser pulse ($BPT^{\bullet+}$)—in air-equilibrated buffer solutions (pH 7.5) containing NaCl (100 mM). B) Arrhenius plot for oxidation of duplex **2d** by $CO_3^{\bullet-}$ radicals. Inset: The transient absorption spectrum of $CO_3^{\bullet-}$ radicals recorded 0.1 ms after the 308 nm laser pulse. The constant k_5 is defined in Table 1.

constant does not depend significantly on the number of G residues, which varies from two to eight bases per duplex. Furthermore, k_5 also does not depend on the guanine sequence contexts sampled here (either isolated, or in groups of two or three contiguous guanines). The previously studied 16-mer self-complementary duplex **11d** (Table 1), with eight Gs,[27] also yields a value of k_5 similar to those observed in the series of the duplexes **1d**–**3d** and **4d**–**7d**. The rate constant for the oxidation of free guanine base—dGMP—is only three times greater than the values for oxidation of duplexes containing multiple guanine residues. Overall, the number and arrangement of guanines in these oligonucleotide duplexes do not seem to affect the electron-transfer rate constants.

Using standard high-resolution gel electrophoresis techniques to detect alkali-labile DNA base damage, we have previously found that $CO_3^{\bullet-}$ radicals can selectively oxidize guanine residues in oligonucleotide duplexes.[27] There is ample evidence from utilization of other DNA oxidants, however, that the yields of alkali-labile guanine oxidation products are higher in ···GG··· and ···GGG··· than in isolated ···G··· sequences.[31,33,40] The lack of a significant base sequence context effect on the magnitude of k_5 for oxidation by $CO_3^{\bullet-}$ radicals of guanines in ···TGT···, ···TGGT···, and ···TGGGT··· sequence contexts (Table 1) is therefore surprising on first consideration.

To demonstrate that the absence of base sequence effects on k_5 is explicitly associated with $CO_3^{\bullet-}$ radicals, we explored the kinetics of G oxidation by an aromatic photosensitizer: the radical cation of the pyrene derivative 7,8,9,10-tetrahydroxytetrahydrobenzo[*a*]pyrene (BPT). This derivative is more soluble than pyrene in aqueous media, and is therefore particularly suitable for studying one-electron transfer phenomena with DNA.[46] The electron-transfer reactions are conveniently triggered by an intense 355 nm laser pulse that induces two-photon ionization of the BPT residues (Table 3).[46] A typical example of a decay curve of the $BPT^{\bullet+}$ radical cation, in a solution containing the duplex **2d** (100 μM), is depicted in Figure 1, and is shown to occur on a timescale of ≈30 μs.

The rate constants of DNA oxidation (k_9, in Table 3) obtained from analysis of the $BPT^{\bullet+}$ decay profiles (measured at the 455 nm maximum of the transient absorption band) recorded in the presence of the oligonucleotide duplexes **1d**–**3d** are compared in Figure 2. The value of k_9 for duplex **3d** (···TGGGT···) is about two times greater than that for duplex **2d** (···TGGT···) and about 40 times greater than in duplex **1d** (···TGT···) (Figure 2). We note that in the case of dGMP the magnitude of k_9 is about 45 times greater than for the single G embedded in duplex **1d** (···TGT···). Reactivity between $BPT^{\bullet+}$ radicals and isolated G residues embed-

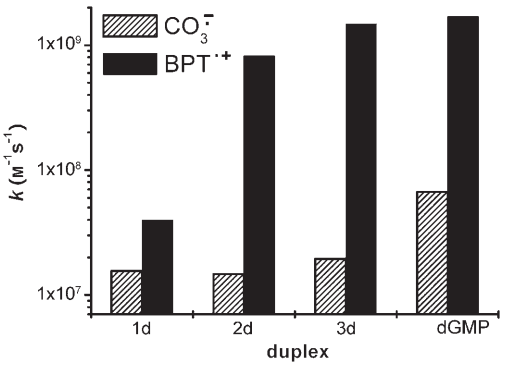

Figure 2. The rate constants for G oxidation in DNA duplexes variously containing a single G base (duplex **1d**), a GG doublet (duplex **2d**), and a GGG triplet (duplex **3d**) by $BPT^{\bullet+}$ and by $CO_3^{\bullet-}$ radicals. The k values were obtained from the best least-squares fits of the appropriate kinetic equations to the transient absorption profiles for decay of $CO_3^{\bullet-}$ (600 nm) and $BPT^{\bullet+}$ (455 nm) recorded in air-equilibrated buffer solutions (pH 7.5) at 23 °C.

ded in double-stranded DNA is considerably reduced in relation to the corresponding value for free dGMP, and this in turn is only about three times smaller than the diffusion-controlled value.[46] In the ···TGGT··· and ···TGGGT··· sequence contexts (Figure 2), however, k_9 approaches the value for dGMP. We note that the $BPT^{\bullet+}$ one-electron transfer rate constant for the oxidation of dGMP is ≈20 times greater than the analogous rate constant—k_5—for the oxidation of dGMP by $CO_3^{\bullet-}$.

Temperature dependence of the $CO_3^{\bullet-}$ one-electron oxidation rate constant k_5: To obtain additional insights into the mechanisms of one-electron oxidation of oligonucleotide duplexes by $CO_3^{\bullet-}$ radicals, we measured the temperature dependence of the rate constants of reactions 5 and 6 (Table 2). In the temperature range of 4–25 °C, the value of the activation energy for the bimolecular disproportionation of $CO_3^{\bullet-}$ radicals (reaction 6) is small and negative ($E_a = -(6\pm3)$ kJ mol^{-1}). This value is in good agreement with the E_a values of $-(8\pm4)$ kJ mol^{-1}[47] and about -7 kJ mol^{-1} estimated from the results of Huie and Clifton.[48] The activation energies obtained for the oxidation of the duplexes **1d–7d** by $CO_3^{\bullet-}$ radicals over the same temperature range are also small, but positive ($E_a = (7\pm3)$ kJ mol^{-1}). The pre-exponential factors (A; $\approx 5\times10^8$ M^{-1}s^{-1}) estimated from this value of E_a are two to three orders of magnitude lower than the typical values of A for a bimolecular reaction,[49] suggesting a complex mechanism for the one-electron oxidation of the oligonucleotide duplexes by $CO_3^{\bullet-}$ radicals (see below).

The polycyclic aromatic radical cation $BPT^{\bullet+}$ has a redox potential of $E^0 \approx 1.5$ V vs. NHE,[50] and is known to readily oxidize dGMP (the midpoint potential at pH 7 is $E_7 = 1.29$ V vs. NHE[51]), but not any of the other three DNA nucleotides, in aqueous solution.[46] The rate constants for oxidation of G in double-stranded oligonucleotides by $BPT^{\bullet+}$ (k_9) are 20 times greater in sequences that contain tandem GG (**2d**)—and 40 times greater in those containing GGG (**3d**)—than in sequence **1d** in which the two guanines are separated from one another (Figure 2). This effect is consistent with the notion[34,35] that guanines in GG and GGG sequences generally have lower ionization potentials than isolated guanines in double-stranded DNA and are therefore more easily oxidizable.

The $CO_3^{\bullet-}$ radical is a one-electron oxidant [$E^0(CO_3^{\bullet-}/CO_3^{2-}) = 1.59$ V vs. NHE[52]] and has been found to oxidize guanines with high selectivity in the sequence d(AAC**G**C-**G**AATTC**G**C**G**TT), which readily forms self-complementary duplexes in aqueous solutions.[27] Although an effect similar to that observed in the case of the $BPT^{\bullet+}$ radical (Figure 2) might have been expected in view of the high oxidation potential of the $CO_3^{\bullet-}$ radical, it is evident that the k_5 value of the electron transfer rate (Table 1) is not particularly sensitive to the presence or absence of guanines. In the case of the $BPT^{\bullet+}$ radical, the value of k_9 does follow the trend k_9(5′-G) < k_9(5′-GG) < k_9(5′-GGG) as predicted by the Saito model[35,42,43] and observed experimentally (Figure 2). However, the one-electron oxidation of the same duplexes by $CO_3^{\bullet-}$ radicals occurs with similar rate constants within the rather narrow range of $(1.5\text{–}3.0)\times10^7$ M^{-1}s^{-1}. These results clearly imply that oxidation of guanines in double-stranded DNA by $CO_3^{\bullet-}$ radicals is governed by different mechanisms than in the case of polycyclic aromatic radical cation one-electron oxidant $BPT^{\bullet+}$.

Electron abstraction from DNA by $CO_3^{\bullet-}$ radicals: The gel electrophoresis cleavage patterns (see below) indicate that the formation of oxidative, alkali-labile guanine lesions is indeed enhanced at guanines in GG and GGG in the sequence contexts of duplexes **9d** and **10d**. However, the rate constants for oxidation of the same sequences by $CO_3^{\bullet-}$ radicals do not vary significantly from one another (Table 1 and Figure 2). In contrast, the rate constants for oxidation by the polycyclic aromatic radical $BPT^{\bullet+}$ are significantly greater for sequences that contain tandem GG or GGG sequences than for those containing isolated guanines (Figure 2). It therefore appears that the rate constants (k_5) for the oxidation of guanines by $CO_3^{\bullet-}$ radicals are sensitive neither to the number of guanines in the duplexes studied, nor to their sequence-context-dependent ionization potentials. We consider the implications of these observations by considering the classical Marcus electron transfer equations, in which the rate constant of electron transfer (k_{el}) is [Eq. (4)]:[53]

$$k_{el} = (\lambda RT)^{-1/2} \exp-[(\Delta G^0+\lambda)^2/4\lambda RT] \quad (4)$$

where λ is the reorganization energy. For large polycyclic aromatic molecules the reorganization energy is of the outer-sphere type and is generally small in the case of reactants with large radii in aqueous solution. In such cases, the electron transfer rate constant is governed by the free energy term ΔG^0, which is proportional to the difference in redox potentials of the electron acceptor and donor couples. This is the case for the oxidation of guanine in oligonucleotides

by the $BPT^{\bullet+}$ radical cations, as the observed rate constant (k_9) is sensitive to decreasing the redox potentials of guanines in GG and GGG sequence contexts.[35,42–44] The observed enhancement of the electron transfer rate k_9 is thus attributed to an enhancement in the driving force ($-\Delta G^0$) of the electron transfer reaction.[53]

The values of k_5 for $CO_3^{\bullet-}$ are one to two orders of magnitude lower than the values of k_9 (Figure 2) characterizing the oxidation of the same duplexes by $BPT^{\bullet+}$ radical cations, even though the two species have similar redox potentials (see above). To explain this difference in the reactivities of $CO_3^{\bullet-}$ and $BPT^{\bullet+}$ radicals toward DNA we propose that the one-electron abstraction from DNA by $CO_3^{\bullet-}$ radicals occurs by an inner-sphere mechanism, in contrast to the outer-sphere mechanisms assumed in the case of $BPT^{\bullet+}$ radicals. Indeed, the rates of electron-transfer reactions involving small inorganic radicals such as $CO_3^{\bullet-}$ and $^{\bullet}NO_2$ by inner-sphere mechanisms are dominated by relatively large reorganization energies. These are generally larger than those involving large polycyclic aromatic molecules and occurring through outer-sphere mechanisms.[46,54] For oxidation of DNA by $CO_3^{\bullet-}$ radicals, this hypothesis is supported by a number of observations:

1) The k_5 values do not vary significantly as a function of the number of contiguous guanines in the case of one-electron oxidation by $CO_3^{\bullet-}$ radicals, suggesting that $\lambda > -\Delta G^0$.
2) The rate constant k_5 exhibits a very weak temperature dependence (Figure 1B) and thus a small activation energy ($E_a = (7 \pm 3)\ kJ\,mol^{-1}$); this in turn suggests that the pre-exponential factors (A; $\approx 5 \times 10^8\ M^{-1}s^{-1}$) for the oxidation of DNA by $CO_3^{\bullet-}$ radicals are also small.
3) The $CO_3^{\bullet-}/CO_3^{2-}$ system is characterized by a very small self-exchange rate constant ($k = 0.4\ M^{-1}s^{-1}$[55]), and hence a high internal reorganization energy, which suggest a low reactivity of $CO_3^{\bullet-}$ radicals in outer-sphere electron transfer reactions.[55] Such an explanation has previously been proposed for electron-transfer reactions of $CO_3^{\bullet-}$ radicals with organic molecules such as ascorbate, tryptophan, cysteine, methionine, etc.[56] The activation energies of these reactions are also small and independent of the driving force of the reaction.

Consistently with an inner-sphere mechanism, the oxidation of individual bases in oligonucleotides by $CO_3^{\bullet-}$ radicals can be described in terms of a simple kinetic scheme involving the formation of an intermediate complex between the oligonucleotide duplexes and the $CO_3^{\bullet-}$ radicals [Eq. (5)]:

$$CO_3^{\bullet-} + \text{oligo} \overset{K_{eq}}{\rightleftharpoons} [CO_3^{\bullet-} \cdots \text{oligo}] \xrightarrow{k_e} \text{oligo}^{\bullet+} + CO_3^{2-} \qquad (5)$$

where K_{eq} ($=k_+/k_-$) is the equilibrium constant and k_e is the rate constant of electron transfer in the complex. If it is assumed that electron transfer is slow ($k_e < k_-$), the rate constant of DNA oxidation, $k_5 = K_{eq}k_e = [\exp(\Delta S_{eq}/R)\ \exp(-\Delta H_{eq}/RT)]\ [A_e\ \exp(-E_e/RT)]$ and the experimentally observed activation energy is determined by the sum of the enthalpy of complex formation ΔH_{eq} and the activation energy of the electron transfer step (E_e). The value of E_e is positive and if ΔH_{eq} is negative, the experimentally observed activation energy E_a can be small, as observed experimentally. A similar mechanistic explanation has previously been suggested by Eriksen et al.[47] for the bimolecular recombination reaction of $CO_3^{\bullet-}$ radicals (reaction 6, Table 2), which is characterized by a small negative activation energy.[47,48] In summary, the abnormally low reactivity of $CO_3^{\bullet-}$ radicals, in spite of their high redox potential, in the oxidation of DNA duplexes is accounted for by an inner-sphere mechanism of the initial electron abstraction step occurring in a weak complex between the oligonucleotide duplexes and the $CO_3^{\bullet-}$ radicals.

Detection of oxidatively damaged bases by piperidine or Fpg treatment and by gel electrophoresis methods: The major products of oxidation of guanine by $CO_3^{\bullet-}$ radicals in double-stranded DNA, the diastereomeric Sp lesions,[28] are alkali-labile and so can be cleaved by the standard hot piperidine treatment;[57,58] Sp lesions can also be excised by the formamidopyrimidine (Fpg) base excision repair glycosylase.[59,60] These cleavage techniques thus represent a simple method for monitoring the base sequence-dependence of Sp product formation.[57,58] In contrast, 8-oxoGua, which is also formed, but in smaller amounts,[28] is not alkali-labile,[61] but can be detected by Fpg treatment.[62] We therefore compared the results of Fpg and hot piperidine treatment on the cleavage patterns of a typical oligonucleotide exposed to $CO_3^{\bullet-}$ radicals to determine whether any hot alkali-resistant lesions had been formed.

The cleavage patterns obtained after exposure of the DNA duplex **6d** to $CO_3^{\bullet-}$ radicals and after standard hot piperidine or Fpg treatment are compared in the gel autoradiographs in Figure 3. Strand cleavage is negligible in the unirradiated control sample with or without the hot piperidine treatment (lanes 1 and 2 in Figure 3A), as is also the case with and without Fpg treatment (lanes 1 and 2 in Figure 3B). Upon irradiation of the same samples, however, Fpg- or hot piperidine-induced cleavage is observed predominantly at the G sites, and the extent of cleavage increases with irradiation time. The overall fraction of cleaved fragments becomes increasingly nonlinear with increasing irradiation time beyond the level of $\approx 10\%$ (Figure 4A), while the photochemical yields of cleaved fragments diminish. The histograms in Figure 3C and 3D show that the distributions of the strand cleavage patterns generated by hot piperidine treatment (Figure 3C) are very close to those produced by the Fpg treatment (Figure 3D). These observations are in agreement with previous findings[28] that the oxidation of oligonucleotides by $CO_3^{\bullet-}$ radicals generates mostly alkali-labile Sp lesions, and that hot piperidine-resistant lesions such as 8-oxoGua[61] are formed only in minor quantities. The kinetics of the total DNA cleavage (Figure 4A) and cleavage at the G sites (Figure 4B) observed in

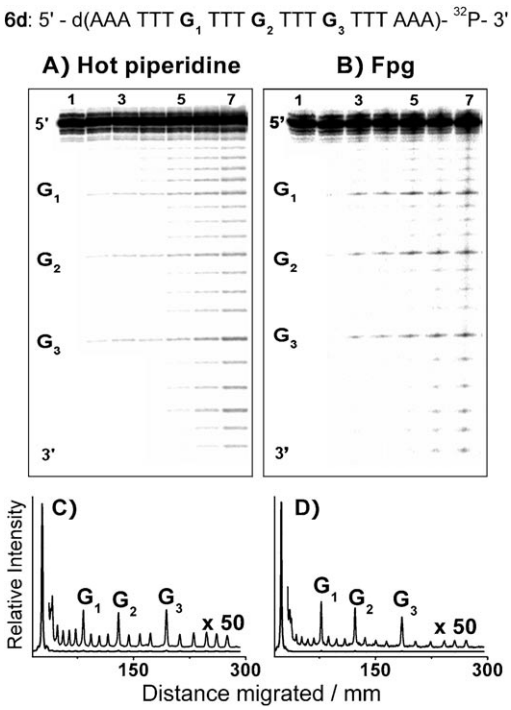

Figure 3. Comparisons of strand cleavage patterns in duplex **6d**, containing three isolated guanines separated by three T bases, after incubation with hot piperidine (A) or with Fpg (B). Autoradiographs of denaturating gels (7 M urea, 20% polyacrylamide gel) showing the cleavage patterns of the duplex **6d** labeled at the 3′-termini and excited by a train of 308 nm laser pulses (20 mJ pulse^{-1} cm^{-2}, 10 pulse s^{-1}) in air-equilibrated buffer solutions (pH 7.5) containing $Na_2S_2O_8$ (10 mM) and $NaHCO_3$ (300 mM). A) Lane 1: unirradiated sequence (without piperidine treatment). Lane 2: unirradiated sequence (after hot piperidine treatment). Lanes 3–7: irradiated sequence (after hot piperidine treatment), irradiated for 5, 10, 15, 30, and 60 s. B) Lane 1: unirradiated sequence (without Fpg treatment). Lane 2 : unirradiated sequence (after Fpg treatment). Lanes 3–7: irradiated sequence (after Fpg treatment), irradiated for 5, 10, 15, 30, and 60 s. The histograms of lanes 4 (in panels A and B) are shown in Panel C (hot piperidine treatment) and Panel D (Fpg treatment).

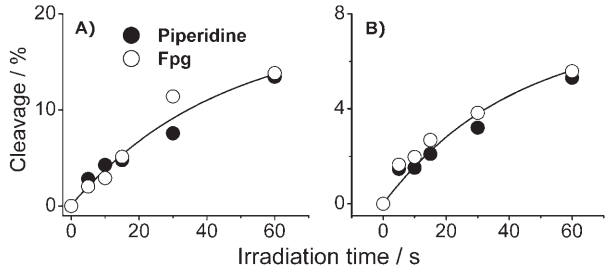

Figure 4. Kinetics of total DNA cleavage (A) and cleavage at G-sites (B) in duplex **6d**, containing three isolated guanines. The cleavage percentages were calculated from the histograms of the autoradiographs of denaturating gels shown in Figure 2.

the experiments with hot piperidine and Fpg treatments are also close to one another. These results indicate that few hot alkali-resistant lesions are formed.

Effects of irradiation time on cleavage patterns: To assess accurately the effects of base sequence context on cleavage patterns in runs of two or three contiguous guanines, it is important to consider the effects of irradiation time. We designed a set of sequences (**4d**, **5d**, **6d**, and **7d**) with guanines at least six base pairs away from the termini in order to avoid end-effects (see below). The 20-mer sequences **4d** and **5d** both contain the same nucleotides in the same proportions, with only two guanines, either separated from one another by six thymidines (**4d**), or adjacent to one another in the center of the duplex (**5d**). Sequences **6d** and **7d** are 21 mer duplexes that each contain three guanines, either separated from one another (**6d**) or grouped together in a contiguous manner (**7d**). These sequences contain as few contiguous guanines as possible (2–3) in order to minimize the complexities of multiple guanines on cleavage patterns discussed in connection with the results shown in Figure 8 (see below). The cleavage patterns for the case of a short irradiation time of 20 s, when the overall level of cleavage is below 20%, are depicted in Figure 5. Interestingly, the

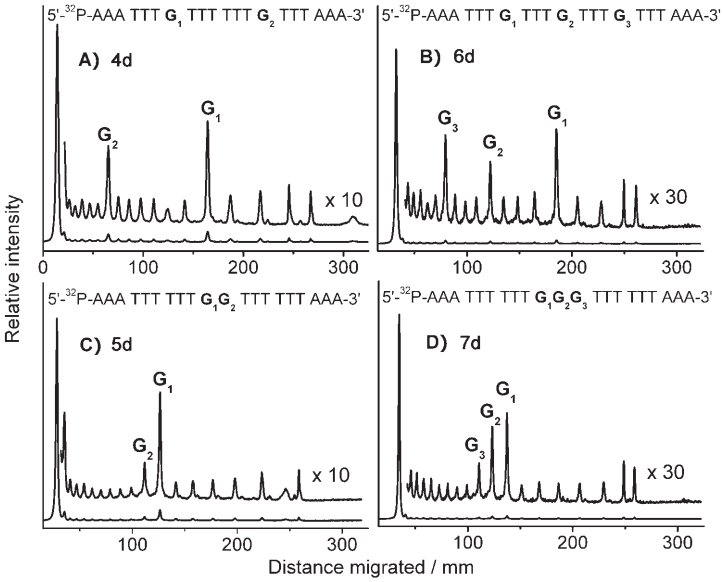

Figure 5. Histograms of the autoradiographs of denaturating gels (7 M urea, 20% polyacrylamide gel) showing the cleavage patterns of the duplexes variously containing two isolated guanines (duplex **4d**, A), a GG doublet (duplex **5d**, C), three isolated guanines (duplex **6d**, B), and a GGG triplet (duplex **7d**, D) excited by a train of 308 nm laser pulses (20 mJ pulse^{-1} cm^{-2}, 10 pulse s^{-1}) in air-equilibrated buffer solutions (pH 7.5) containing $Na_2S_2O_8$ (10 mM) and $NaHCO_3$ (300 mM) and treated with hot piperidine.

levels of damage at the isolated guanine sites in sequences **4d** and **6d** (Figure 5A and 5C) are similar to those in the sequence context of **8d** (Figure 8A, see below), possessing additional G residues near the ends of the duplexes. However, the relative distribution of the cleavage patterns in the contiguous guanines in sequence **7d** is $G_1 > G_2 > G_3$ (Figure 5D), which is different from the distribution in the 5′···GGG··· sequences in duplex **10d** (see below). The per-

centages of sequences cleaved at the different G positions and adjacent T residues as a function of irradiation time are summarized in Figure 6A and Figure 7A for the 5′-

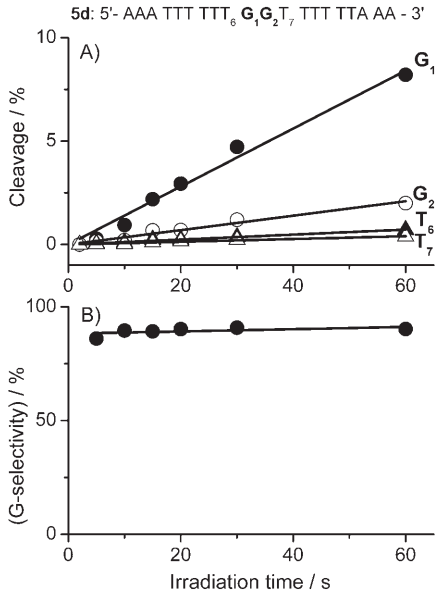

Figure 6. Kinetics of cleavage at G-sites and adjacent thymidines in duplex **5d**, containing two contiguous guanines. The cleavage selectivities at the contiguous guanines were calculated as the area ratios under the G_1 and G_2 peaks and under the T_6, G_1, G_2, and T_7 peaks.

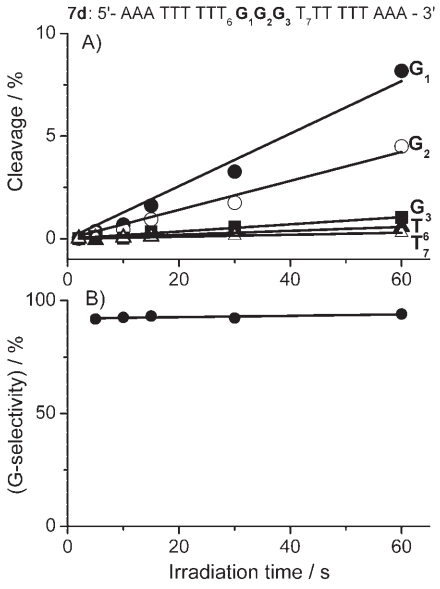

Figure 7. Kinetics of cleavage at G-sites and adjacent thymidines in duplex **7d**, containing three contiguous guanines. The cleavage selectivities at the contiguous guanines were calculated as the area ratios under the G_1, G_2, and G_3 peaks and under the T_6, G_1, G_2, G_3, and T_7 peaks.

···$T_6G_1G_2T_7$··· (**5d**) and 5′-···$T_6G_1G_2G_3T_7$··· (**7d**) duplexes, respectively. The yields of alkali-labile lesions are approximately linear up to irradiation times of 60 s for G_2, G_3, T_6, and T_7. Using data points shown in Figure 6A and Figure 7A we estimated the cleavage selectivities at the contiguous guanines. The areas under the G_1 and G_2 peaks in **5d** and the G_1, G_2, and G_3 peaks in **7d** were summed and compared with the results of cleavage at the $T_6G_1G_2T_7$ and $T_6G_1G_2G_3T_7$ fragments with adjacent T residues. The cleavage yield within the contiguous guanines increases linearly and comprises nearly 90% of the total cleavage (only ≈10% at all of the T residues) up to irradiation times of 60 s (Figure 6B and Figure 7B). The relative reactivities of the different G bases in the duplexes **5d** and **7d** were determined from the initial rates of the G cleavage (Figure 6 and Figure 7. In duplex **5d** the ratio of the initial rates of G_1 and G_2 oxidation is 4.1:1, while in the duplex **7d** the ratio of the initial rates of G_1, G_2, and G_3 oxidation sites is 12:6.5:1, so damage at G is dominant in the duplexes studied under our reaction conditions.

Reactivities of guanines in different sequence contexts with $CO_3^{\bullet-}$ radicals: The observed cleavage patterns can deviate from the true patterns because of ^{32}P-end-labeling effects when the same oligonucleotide has more than one alkali-labile damaged base. In that case, only the damaged base closest to the ^{32}P-label can be detected. Since $CO_3^{\bullet-}$ radicals also cause damage at thymidine sites, these issues must be considered in comparison of cleavage efficiencies at different guanines in the same oligonucleotide sequence. For these reasons, sequence-dependent cleavage patterns must be evaluated as a function of irradiation time, to ensure that the experiments are confined to the linear response region (Figures 5–8). Furthermore, we had reported previously that guanine residues closer to the ends of the duplexes were oxidized by $CO_3^{\bullet-}$ radicals more extensively than guanines closer to the center of the duplexes.[27] Here we characterize these end-effects in greater detail.

Effects of solvent exposure on reactivities of guanine in DNA with $CO_3^{\bullet-}$ radicals—end-effects: The duplexes **8d**, **9d**, and **10d** were designed to evaluate the influence of end-effects on cleavage patterns through the positioning of single guanines surrounded by thymidines close to both ends of these duplexes. When guanine lesions are positioned at the ends—or close to the ends—of oligonucleotide duplexes, strikingly higher oxidative guanine cleavage levels are observed at these positions than at guanines in the interior of the duplexes. This effect is demonstrated in Figure 8 with duplexes **8d**, **9d**, and **10d**; in each case the third nucleotide counted either from the 5′- or from the 3′-end is a single guanine. In all cases the most efficient cleavage is detected at these two guanines and is higher than the damage at the contiguous ···GG··· and ···GGG··· guanine sequences in duplexes **9d** and **10d**, respectively. The cleavage at all inner bases is thus significantly less. The increased damage at guanines close to the two ends of the duplexes is attributed to increased solvent exposure, and thus greater reactivity of these guanines with $CO_3^{\bullet-}$ radicals. This greater solvent exposure is due to strand-fraying effects that correspond to

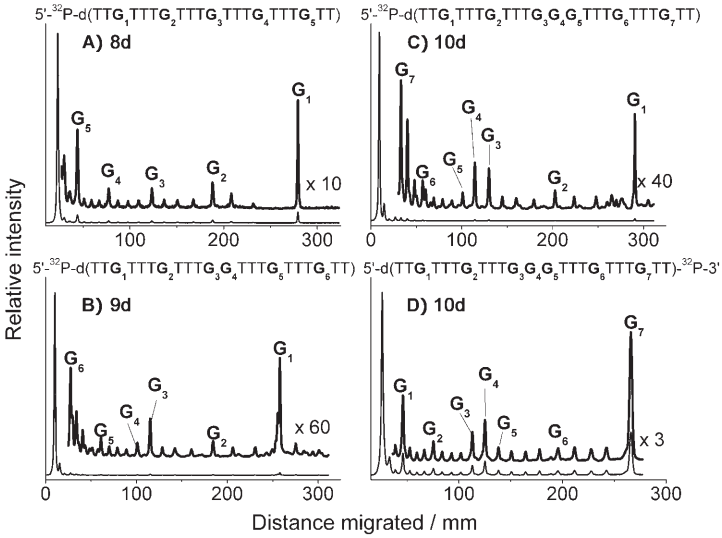

Figure 8. Histograms of the autoradiographs of denaturating gels (7 M urea, 20% polyacrylamide gel) showing the cleavage patterns of the duplexes variously containing five isolated guanines (duplex **8d**, 5′-end-labeled, A), four isolated guanines and a GG doublet (duplex **9d**, 5′-end-labeled, B), and four isolated guanines and a GGG triplet (duplex **10d**, 5′-end-labeled, C) and duplex **10d** (3′-end-labeled, D), excited by a train of 308 nm laser pulses (20 mJ pulse^{-1} cm^{-2}, 10 pulse s^{-1}) in air-equilibrated buffer solutions (pH 7.5) containing $Na_2S_2O_8$ (10 mM) and $NaHCO_3$ (300 mM) and treated with hot piperidine.

weakening of the Watson–Crick hydrogen bonding and a greater probability of opening of base pairs.[63] Such greater reactivity of partially solvent-exposed guanine residues is also consistent with the greater reactivity—by factors of 4–5—of identical sequences in either the single-stranded or double-stranded forms (data not shown).

Effects of separated and contiguous guanine residues on strand cleavage patterns: To evaluate the effects on reactivity and cleavage yields and patterns of contiguous guanines within the inner regions of the duplexes, we designed oligonucleotide duplexes **8d**, **9d**, and **10d** (Table 1). These duplexes were designed for intercomparison of cleavage at *single* guanines and in runs of *two* or *three* nearby contiguous guanines on the same strand. In each of these duplexes the guanines closest to the two termini are not utilized in these comparisons because of the end-effects described above. The guanines G_3 in **8d**, G_3G_4 in **9d**, and $G_3G_4G_5$ in **10d** (counted from the 5′-end; see numbering scheme in Figure 8) are all positioned in the centers of the duplexes and distant from the ends, so that the differences in intrinsic cleavage patterns can be observed. Indeed, the levels of cleavage at G_2, G_3, and G_4 in duplex **8d** are similar, confirming that end-effects are no longer important for guanines positioned in the inner region of this duplex. These experiments were conducted at relatively low irradiation dosages to minimize distortions of the cleavage patterns due to multiply damaged guanine residues on the same strand. We first note that, even at low dosages, there is observable cleavage at T residues, and that the cleavage at the interior single guanines G_2, G_3, and G_4 in **8d**, at G_2 and G_5 in **9d**, and at G_2 and G_6 in **10d** is larger than the extent of damage observed at neighboring T sites by a factor of only 2–3 (Figure 8). Moreover, the cleavage at the 3′-contiguous guanines G_4 in the 5′-···TG_3G_4T··· sequence context of **9d** (Figure 8B) and G_5 in the 5′-···$TG_3G_4G_5T$··· sequence context of **10d** (Figure 8C) occur with significantly lower efficiencies than at the one or two, respectively, 5′-flanking guanines. The cleavage efficiencies are higher at the 5′-side guanine G_3 in the 5′-···TG_3G_4T··· sequence context of **9d** and at the central guanine G_4 in the 5′-···$TG_3G_4G_5T$··· sequence context of duplex **10d** (Figure 8B, C, and D). In all cases, the extent of cleavage in runs of two or three guanines is the smallest at the 3′-G. We note here that the order of reactivities in the 5′-···$TG_3G_4G_5T$··· sequence context of duplex **10d** is $G_4 > G_3 > G_5$ (Figure 8C) and that this order of reactivities is different from that observed in duplex **7d** (Figure 5D), where the guanine at the 5′-end exhibits the highest reactivity. We attribute this difference to the overall sequence context, since in duplex **10d** there are other nearby guanines that can exchange holes with guanines in the 5′-···GGG··· sequence, whereas in duplex **5d** there are no other guanines present.

It is important to verify that the cleavage patterns in runs of guanines are not the result of distortions of the intrinsic cleavage patterns arising from the ^{32}P-end-labeling effects. We therefore compared the cleavage patterns in duplexes **10d**, with the guanine-containing strand ^{32}P-end-labeled either at its 5′- (Figure 8C) or at its 3′-end (Figure 8D). Similar cleavage patterns are observed in each case, with the 3′-side G_5 in each ···$G_3G_4G_5$··· triplet in **10d** exhibiting the lowest cleavage efficiency. Overall, the results shown in Figure 5 are in excellent agreement with previous observations by other workers, who used a variety of oxidizing agents to generate hot alkali-sensitive guanine lesions in 5′-···TGG···[30–35,37] and 5′-···TGGG···[35,36,39,64] sequences in different oligonucleotide duplexes. Furthermore, these observations are also consistent both with the Saito model of hole transfer and hole distributions among the different guanines in runs of two or three guanines,[35,42,43] and also with the results of more recent calculations.[44]

The seeming paradox between sequence-independent hole injection rates and sequence-dependent chemical product formation and cleavage patterns: Although the initial rate constant of one-electron oxidation of guanine by $CO_3^{\bullet-}$ radical anions in the oligonucleotides studied here does not follow the Saito relationships, the distributions of the damaged, hot alkali-labile guanines are in full agreement with this model. These results are consistent with a primary one-electron abstraction rate constant, or hole injection, that is independent of guanine base sequence context for the reasons already discussed. Once the hole is injected, it can migrate between the different guanines across thymidine bridges if the donor and acceptor are close enough to one another,[65–67] and eventually become trapped at the lowest-energy sites: the contiguous ···GG··· or ···GGG··· sequen-

ces.[30–37,39] In any case, even if the guanine residues are spaced too far apart for efficient hole transfer to take place, a hole injected into a particular set of two or three contiguous guanines will redistribute itself according to patterns dictated by the neighboring base sequence context and solvent environment.[35,44] This redistribution of the hole density occurs before the subsequent chemical reactions that ultimately result in the formation of the hot piperidine-labile spiroiminodihydantoin lesions can take place,[28,29] giving rise to the observed sequence-dependent cleavage patterns. Since we clearly observe sequence-dependent rate constants with the $BPT^{\bullet+}$ radical cation (Figure 2), as well as cleavage patterns similar to those observed in the case of the $CO_3^{\bullet-}$ radical anion (unpublished observations), it is indeed possible to observe a correlation between the primary one-electron oxidation rate constant and ultimate product formation. However, we have shown here that such a correlation is not absolutely required, as exemplified by the oxidation of guanines in DNA by the $CO_3^{\bullet-}$ radical anion. Whatever the mechanism of hole injection, the holes redistribute themselves among the lowest-energy guanines in runs of guanines, so a sequence-dependent product distribution should be observable even when the initial one-electron transfer step is not sequence-dependent, because any injected hole will be redistributed over the available guanines in contiguous G sequences. Essentially, the processes of hole injection and cleavage patterns are decoupled; the distribution of chemical end-products is a relative measurement that involves the reactivities of guanine radicals in the same DNA strand and is independent of the rate of hole injection. The efficiency of the initial one-electron transfer oxidation step can influence the overall photochemical yield but not the product distribution among different sites in runs of guanines.

Comparisons of sequence-dependent cleavage by nitrosoperoxycarbonate and by $CO_3^{\bullet-}$ radical anion: Our group has recently shown that the oxidation of guanines by the nitrosoperoxycarbonate anion (i.e., the formation of hot alkali-labile or Fpg labile sites) does not follow the sequence dependence predicted by the Saito model.[35,42,43] Interestingly, it was found that the ratio of (alkali-labile)/(Fpg-labile) damage was also dependent on the bases flanking the damaged guanines. Our results reported here have established that the $CO_3^{\bullet-}$ radical anion, a decomposition product of $ONOOCO_2^-$, does not by itself account for the different sequence dependence observed in the case of nitrosoperoxycarbonate. In the latter case, the chemical end-products are formed by other pathways that most probably involve $^{\bullet}NO_2$ and possibly other reactions that result in the unusual sequence-dependent cleavage patterns and product ratios reported.[36,42] Indeed, the spectrum of products and mutations associated with the decomposition of peroxynitrite in the absence or presence of bicarbonate is quite complex.[22,25,26] The next stage of research, with the objectives of gaining better understanding of base sequence-dependent reactions of peroxynitrite and nitrosoperoxycarbonate with DNA,[29] will involve studies of the effects of mixtures of $^{\bullet}NO_2$ and $CO_3^{\bullet-}$ radicals for the role of base sequence context on DNA product formation and cleavage patterns.

Conclusion

Carbonate radicals oxidize guanine in DNA by a one-electron abstraction reaction that, through a series of subsequent oxidation steps and chemical reactions, culminates in the formation of guanine oxidation products (mainly the hot alkali- and Fpg-labile spiroiminodihydantoin lesions). From previous work,[35,36,43] a higher rate constant for the initial $CO_3^{\bullet-}$-mediated electron transfer step (k_5) was anticipated in duplexes containing ···GG··· and ···GGG··· sequences. Paradoxically, though, k_5 for the oxidation of guanine in DNA by $CO_3^{\bullet-}$ radicals exhibits only small variations within a narrow interval $[(1.5–3.0)\times10^7\,M^{-1}s^{-1}]$ in these sequence contexts. On the other hand, the distributions of oxidized guanine end-products at different guanine bases within contiguous ···GG··· and ···GGG··· sequences are significantly higher at the 5′-G in ···GG··· and at the two 5′-GG bases in the ···GGG··· sequence contexts, as expected from the Saito model.[35,42,43] This apparent paradox is attributed to 1) the lack of dependence of k_5 on sequence context, indicating that the one-electron oxidation of guanine in DNA by $CO_3^{\bullet-}$ radicals occurs by way of an inner-sphere mechanism with a large reorganization energy, and 2) in the case of the sequence-dependent chemical product distributions, a combination of initial hole distributions among the contiguous guanines and the subsequent differences in chemical reaction yields at each guanine.

Experimental Section

Materials: All organic solvents and inorganic salts were obtained from Sigma–Aldrich Fine Chemicals and were used as received; Fpg protein was obtained from New England BioLabs (Ipswich, MA). The oligonucleotides were synthesized by standard automated phosphoramidite chemistry techniques. Phosphoramidites and other chemicals required for oligonucleotide synthesis were obtained from Glen Research (Sterling, VA). The tritylated oligonucleotides were deprotected overnight at 55 °C by treatment with concentrated aqueous ammonia solutions. The crude oligonucleotides were purified by reversed-phase HPLC, detritylated in 80 % acetic acid by standard procedures, and desalted by reversed-phase HPLC. The integrities of the oligonucleotides were confirmed by MALDI-TOF mass spectrometry. The damaged strands present in minor quantities in the oligonucleotide samples were digested by a standard hot piperidine treatment[68] and removed by polyacrylamide gel electrophoresis. A pyrene derivative with enhanced water solubility—7,8,9,10-tetrahydroxytetrahydrobenzo[a]pyrene (BPT)—was prepared by hydrolysis of racemic *anti*-BPDE (7*r*,8*t*-dihydroxy-*t*9,10*t*-epoxy-7,8,9,10-tetrahydrobenzo[*a*]pyrene, a gift from Dr. S. Amin, American Health Foundation, Valhalla, NY), and purified by reversed-phase HPLC. The concentrations of BPT in the sample solutions were generally $\approx10\,\mu M$ as estimated from the molar extinction coefficient of BPT ($\varepsilon_{343}=2.9\times10^4\,M^{-1}\,cm^{-1}$[46]).

Laser flash photolysis and measurements of electron transfer rates: The kinetics of oxidative reactions initiated by free radicals were monitored directly by use of a fully computerized kinetic spectrometer system (≈7 ns response time) described elsewhere.[69] The 0.4×1 cm quartz cell

(0.25 mL sample volume) was thermostated inside a copper holder fitted with a circulating water jacket. The transient absorbance was probed along a 1 cm optical path with a light beam (75 W xenon arc lamp) oriented perpendicular to the laser beam. The signal was detected with a Hamamtsu 928 photomultiplier tube and recorded with a Tektronix TDS 5052 oscilloscope operating in its high-resolution mode, which provided a satisfactory signal/noise ratio after a single laser shot. The rate constants were determined by least squares fits of the appropriate kinetic equations to the experimentally measured transient absorption profiles as described in detail elsewhere.[28,46] The values reported are averages of five independent measurements.

The $CO_3^{\bullet-}$ radicals were generated by two consecutive reactions that begin with the photodissociation of persulfate anions into $SO_4^{\bullet-}$ radical anions (reaction 1, Table 2) induced by intense 308 nm nanosecond XeCl

Table 2. Reaction scheme for DNA oxidation by $CO_3^{\bullet-}$ radicals.

No.	Reaction	k_n [$M^{-1}s^{-1}$]
1	$S_2O_8^{2-}+h\nu \rightarrow 2SO_4^{\bullet-}$	$\varphi_{308}=0.55$ (Ref. [72])
2	$SO_4^{\bullet-}+SO_4^{\bullet-} \rightarrow S_2O_8^{2-}$	$(1.1\pm0.1)\times10^9$ (Ref. [27])
3	$SO_4^{\bullet-}+oligo \rightarrow$	$(3.2\pm0.3)\times10^9$ (Ref. [28])
4	$SO_4^{\bullet-}+HCO_3^- \rightarrow SO_4^{2-}+CO_3^{\bullet-}$	$(4.6\pm0.5)\times10^6$ (Ref. [27])
5	$CO_3^{\bullet-}+oligo \rightarrow$	$(0.6–2.4)\times10^7$ (Ref. [28])
6	$CO_3^{\bullet-}+CO_3^{\bullet-} \rightarrow C_2O_6^{2-} \rightarrow CO_4^{2-}+CO_2$	$(1.3\pm0.1)\times10^7$ (Ref. [27])

excimer laser pulses. In turn, the $SO_4^{\bullet-}$ radicals, detectable because of their characteristic absorption band at 455 nm with an extinction coefficient[70] of 1600 $M^{-1}cm^{-1}$, oxidize bicarbonate anions into $CO_3^{\bullet-}$ radical anions (reaction 1, Table 2). The $CO_3^{\bullet-}$ radicals thus formed were directly monitored by the appearance of their characteristic absorption band at 600 nm, with an extinction coefficient[71] of 1970 $M^{-1}cm^{-1}$. The $SO_4^{\bullet-}$ radicals can also oxidize the DNA bases,[27,28] and both the $SO_4^{\bullet-}$ and the $CO_3^{\bullet-}$ radicals can undergo recombination (reactions 2 and 6). It is therefore important to optimize the reaction conditions in order to allow predominant observation of the reaction kinetics of electron transfer between $CO_3^{\bullet-}$ radicals and the oligonucleotide strands.

The optimal conditions[27,28] were determined by considering the set of rate constants listed in Table 2. To minimize the contribution of the reactions of $SO_4^{\bullet-}$ radicals with oligonucleotides (reaction 3 in Table 2), we used high concentrations of HCO_3^- (300 mM) and much lower concentrations of oligonucleotides ($\leq$0.1 mM). Under these conditions the contribution of the direct oxidation of the oligonucleotides by $SO_4^{\bullet-}$ radicals—determined from the ratio of the pseudo first-order rate constants, k_3[oligo]/(k_4[HCO_3^-]+k_3[oligo])—can be estimated. In the spectroscopic transient absorption experiments a high oligonucleotide concentration (100 μM) was required in order to maximize the signal/noise ratio. Under these conditions, the k_3[oligo]/(k_4[HCO_3^-]+k_3[oligo]) ratio was $\approx$0.2, and so $\approx$20% of the DNA oxidation events occurred through the $SO_4^{\bullet-}$ radicals. This did not influence the measurements of the rates of DNA oxidation by $CO_3^{\bullet-}$ radicals on submillisecond timescales ($\tau=1/k_5$[oligo]$=$0.4–1.7 ms), however, since the $SO_4^{\bullet-}$ radical reactions occur on much faster timescales ($\tau=1/\{k_3$[oligo]+k_4[HCO_3^-]$\}\approx$0.6 μs (Table 2).

In the experiments with BPT as the photosensitizer, the samples were excited by use of a 355 nm nanosecond Nd:Yag laser. The relevant and important steps leading to the oxidation of oligonucleotides are summarized in Table 3.

Intense 355 nm nanosecond laser pulse excitation induces two-photon ionization of the pyrene-like BPT aromatic residues (reaction 7, Table 3) to form the $BPT^{\bullet+}$ radical cations and hydrated electrons.[46,73] In the presence of oxygen, the hydrated electrons are rapidly scavenged by O_2 to form superoxide radical anions (reaction 8, Table 3) that do not react directly with DNA.[75] The $BPT^{\bullet+}$ radicals can thus be used to oxidize individual bases in oligonucleotides (reaction 9, , Table 3).

Table 3. Reaction scheme for DNA oxidation by $BPT^{\bullet+}$ radicals.

No.	Reaction	k_n [$M^{-1}s^{-1}$]
7	$BPT+2h\nu \rightarrow BPT^{\bullet+}+e^-$	(Refs. [46,73])
8	$e^-+O_2 \rightarrow O_2^{\bullet-}$	1.9×10^{10} (Ref. [74])
9	$BPT^{\bullet+}+oligo \rightarrow$	$(0.04–2)\times10^9$

Preparation of ^{32}P-end-labeled oligonucleotides for strand cleavage assays: The oligonucleotide strands ($\approx$50 pmol) were labeled at their 5′-termini by treatment with OptiKinase (USB, Cleveland, Ohio) and [γ-^{32}P]ATP (Perkin–Elmer Life and Analytical Sciences, Boston, MA) at 37 °C for 30 min. Labeling at the 3′-termini was achieved by treatment with terminal deoxynucleotidyl transferase (Fermentas Inc., Hanover, MD) and [α-^{32}P]ddATP (Amersham Bioscience Corp. Piscataway, NJ). The labeled samples were purified by polyacrylamide gel electrophoresis and exposed to Kodak X-OMAT AR film (Eastman Kodak Co., Rochester, NY), and the required bands were cut out and soaked overnight in an elution buffer (0.5 M ammonium acetate, 0.01 M magnesium diacetate, 0.4 mL). Pure oligonucleotides from the extracted samples were isolated by standard ethanol precipitation. The samples used in the photocleavage experiments were prepared by mixing "cold" and radiolabeled strands to obtain $\approx$50 μL of the oligonucleotide with final concentrations of $\approx$100 μM. The DNA duplexes were prepared by annealing the two strands in phosphate buffer solution (pH 7, 20 mM) containing NaCl (0.1 M) at 90 °C for 2 min, and then allowing the samples to cool slowly back to room temperature overnight.

Polyacrylamide DNA strand cleavage assay: The samples of duplexes (10 μL, $\approx$10 μM) containing ^{32}P-5′- or -3′-end labeled strands in 2×2 mm square Pyrex capillary tubes (Vitrocom, Inc., Mountain Lakes, NJ) were irradiated with 308 nm or 355 nm laser pulses ($\approx$20 mJ $pulse^{-1}cm^{-2}$, 10 Hz). After the irradiation, the reaction mixture was quenched by addition of β-mercaptoethanol (1 μL, 0.1 M) solution (or 0.1 M $Na_2S_2O_4$). To reveal oxidatively modified DNA bases, the irradiated samples were treated either with hot piperidine or with the glycosylase Fpg to induce strand breaks. The irradiated samples were mixed with piperidine (100 μL, 1 M), heated at 90 °C for 30 min, and vacuum-dried, and piperidine traces were removed by repeated lyophilization (twice).

Alternatively, the irradiated sample (5 μL) was incubated at 37 °C in a Tris-HCl buffer solution (pH 7.5, 50 μL, 20 mM) containing Fpg (0.9 μM), EDTA (0.5 mM), NaCl (50 mM), and BSA (0.1 mg mL^{-1}). After 30 or 60 min the reaction was terminated by the addition of an equal volume of formamide denaturing loading buffer (95% formamide, 0.025% xylene cyanole, and 0.025% bromophenol blue in sterilized water).

The cleaved oligonucleotide fragments were resolved on a 20% denaturing acrylamide/bisacrylamide (19:1) gel containing urea (7 M) on a 38×50 cm Sequi-Gen cell (Bio-Rad, Melville, NY). The vacuum-dried gels were quantitatively assayed by use of a Storm 840 Phosphorimager system (GE Healthcare). The extent of cleavage was estimated from densitometric traces of the autoradiograms with the aid of a Storm 840 software package. Here we investigated in detail the cleavage patterns of double-stranded oligonucleotides exposed to oxidation by $CO_3^{\bullet-}$ radicals in air-saturated solutions. In these experiments the oligonucleotide duplex concentration was only 10 μM, so $\approx$98% of the observed cleavage was the result of the oxidation of the oligonucleotides by $CO_3^{\bullet-}$ rather than by $SO_4^{\bullet-}$ radicals (see above). The fractions of cleaved oligonucleotide strands were kept below 20% to minimize nonlinear effects.[33]

Acknowledgements

This work was supported by the National Institutes of Health, Grants 1 R01 CA110261 and CA26735 (to P.C.D.), and by a grant from the Kresge Foundation. Young-Ae Lee gratefully acknowledges support from the Post-Doctoral Fellowship Program of the Korean Science and Engineering Foundation. Components of this work were conducted in the Shared Instrumentation Facility at NYU that was constructed with support from Research Facilities Improvement Grant C06 RR-16572 from the National Center for Research Resources, NIH.

[1] F. Balkwill, K. A. Charles, A. Mantovani, *Cancer Cell* **2005**, *7*, 211–217.
[2] A. M. De Marzo, T. L. DeWeese, E. A. Platz, A. K. Meeker, M. Nakayama, J. I. Epstein, W. B. Isaacs, W. G. Nelson, *J. Cell. Biochem.* **2004**, *91*, 459–477.
[3] L. M. Coussens, Z. Werb, *Nature* **2002**, *420*, 860–867.
[4] F. Balkwill, A. Mantovani, *Lancet* **2001**, *357*, 539–545.
[5] H. Kuper, H. O. Adami, D. Trichopoulos, *J. Intern. Med.* **2000**, *248*, 171–183.
[6] M. B. Grisham, D. Jourd'heuil, D. A. Wink, *Aliment. Pharmacol. Ther.* **2000**, *14 Suppl. 1*, 3–9.
[7] L. J. Marnett, *Carcinogenesis* **2000**, *21*, 361–370.
[8] L. J. Marnett, *Toxicology* **2002**, *181–182*, 219–222.
[9] P. C. Dedon, S. R. Tannenbaum, *Arch. Biochem. Biophys.* **2004**, *423*, 12–22.
[10] J. S. Beckman, T. W. Beckman, J. Chen, P. A. Marshall, B. A. Freeman, *Proc. Natl. Acad. Sci. USA* **1990**, *87*, 1620–1624.
[11] H. Ischiropoulos, L. Zhu, J. S. Beckman, *Arch. Biochem. Biophys.* **1992**, *298*, 446–451.
[12] H. Ischiropoulos, J. S. Beckman, *J. Clin. Invest.* **2003**, *111*, 163–169.
[13] K. L. Davis, E. Martin, I. V. Turko, F. Murad, *Annu. Rev. Pharmacol. Toxicol.* **2001**, *41*, 203–236.
[14] R. E. Huie, S. Padmaja, *Free Radical Res. Commun.* **1993**, *18*, 195–199.
[15] R. Kissner, T. Nauser, P. Bugnon, P. G. Lye, W. H. Koppenol, *Chem. Res. Toxicol.* **1997**, *10*, 1285–1292.
[16] S. V. Lymar, J. K. Hurst, *J. Am. Chem. Soc.* **1995**, *117*, 8867–8868.
[17] G. Merenyi, J. Lind, *Chem. Res. Toxicol.* **1997**, *10*, 1216–1220.
[18] S. Goldstein, G. Czapski, *J. Am. Chem. Soc.* **1999**, *121*, 2444–2447.
[19] G. R. Hodges, K. U. Ingold, *J. Am. Chem. Soc.* **1999**, *121*, 10695–10701.
[20] M. G. Salgo, K. Stone, G. L. Squadrito, J. R. Battista, W. A. Pryor, *Biochem. Biophys. Res. Commun.* **1995**, *210*, 1025–1030.
[21] C. Szabo, B. Zingarelli, M. O'Connor, A. L. Salzman, *Proc. Natl. Acad. Sci. USA* **1996**, *93*, 1753–1758.
[22] N. Y. Tretyakova, S. Burney, B. Pamir, J. S. Wishnok, P. C. Dedon, G. N. Wogan, S. R. Tannenbaum, *Mutat. Res.* **2000**, *447*, 287–303.
[23] S. Burney, J. C. Niles, P. C. Dedon, S. R. Tannenbaum, *Chem. Res. Toxicol.* **1999**, *12*, 513–520.
[24] S. Burney, J. L. Caulfield, J. C. Niles, J. S. Wishnok, S. R. Tannenbaum, *Mutat. Res.* **1999**, *424*, 37–49.
[25] M. J. Juedes, G. N. Wogan, *Mutat. Res.* **1996**, *349*, 51–61.
[26] B. Pamir, G. N. Wogan, *Chem. Res. Toxicol.* **2003**, *16*, 487–492.
[27] V. Shafirovich, A. Dourandin, W. Huang, N. E. Geacintov, *J. Biol. Chem.* **2001**, *276*, 24621–24626.
[28] A. Joffe, N. E. Geacintov, V. Shafirovich, *Chem. Res. Toxicol.* **2003**, *16*, 1528–1538.
[29] C. Crean, N. E. Geacintov, V. Shafirovich, *Angew. Chem.* **2005**, *117*, 5185–5188; *Angew. Chem. Int. Ed.* **2005**, *44*, 5057–5060.
[30] D. B. Hall, R. E. Holmlin, J. K. Barton, *Nature* **1996**, *382*, 731–735.
[31] M. E. Nunez, D. B. Hall, J. K. Barton, *Chem. Biol.* **1999**, *6*, 85–97.
[32] D. Ly, Y. Kan, B. Armitage, G. B. Schuster, *J. Am. Chem. Soc.* **1996**, *118*, 8747–8748.
[33] G. B. Schuster, *Acc. Chem. Res.* **2000**, *33*, 253–260.
[34] I. Saito, M. Takayama, H. Sugiyama, K. Nakatani, A. Tsuchida, M. Yamamoto, *J. Am. Chem. Soc.* **1995**, *117*, 6406–6407.
[35] I. Saito, T. Nakamura, K. Nakatani, Y. Yoshioka, K. Yamaguchi, H. Sugiyama, *J. Am. Chem. Soc.* **1998**, *120*, 12686–12687.
[36] Y. Yoshioka, Y. Kitagawa, Y. Takano, K. Yamaguchi, T. Nakamura, I. Saito, *J. Am. Chem. Soc.* **1999**, *121*, 8712–8719.
[37] K. Nakatani, C. Dohno, I. Saito, *J. Am. Chem. Soc.* **1999**, *121*, 10854–10855.
[38] E. Meggers, D. Kusch, M. Spichty, U. Wille, B. Giese, *Angew. Chem.* **1998**, *110*, 474–476; *Angew. Chem. Int. Ed.* **1998**, *37*, 460–462.
[39] E. Meggers, M. E. Michel-Beyerle, B. Giese, *J. Am. Chem. Soc.* **1998**, *120*, 12950–12955.
[40] B. Giese, *Acc. Chem. Res.* **2000**, *33*, 631–636.
[41] B. Giese, *Annu. Rev. Biochem.* **2002**, *71*, 51–70.
[42] H. Sugiyama, I. Saito, *J. Am. Chem. Soc.* **1996**, *118*, 7063–7068.
[43] Y. Yoshioka, H. Kawai, T. Sato, K. Yamaguchi, I. Saito, *J. Am. Chem. Soc.* **2003**, *125*, 1968–1974.
[44] K. Senthilkumar, F. C. Grozema, C. F. Guerra, F. M. Bickelhaupt, L. D. A. Siebbeles, *J. Am. Chem. Soc.* **2003**, *125*, 13658–13659.
[45] Y. Margolin, J. F. Cloutier, V. Shafirovich, N. E. Geacintov, P. C. Dedon, *Nat. Chem. Biol.* **2006**, *2*, 365–366.
[46] V. A. Kuzmin, A. Dourandin, V. Shafirovich, N. E. Geacintov, *Phys. Chem. Chem. Phys.* **2000**, *2*, 1531–1535.
[47] T. E. Eriksen, J. Lind, G. Merenyi, *Radiat. Phys. Chem.* **1985**, *26*, 197–199.
[48] R. E. Huie, C. L. Clifton, *J. Phys. Chem.* **1990**, *94*, 8561–8567.
[49] R. E. Weston, H. A. Schwarz, *Chemical Kinetics*, Prentice–Hall, Englewood Cliffs, NJ, **1972**, pp. 1–274.
[50] V. Y. Shafirovich, S. H. Courtney, N. Ya, N. E. Geacintov, *J. Am. Chem. Soc.* **1995**, *117*, 4920–4929.
[51] S. Steenken, S. V. Jovanovic, *J. Am. Chem. Soc.* **1997**, *119*, 617–618.
[52] R. E. Huie, C. L. Clifton, P. Neta, *Radiat. Phys. Chem.* **1991**, *38*, 477–481.
[53] R. A. Marcus, N. Sutin, *Biochim. Biophys. Acta* **1985**, *811*, 265–320.
[54] V. Shafirovich, J. Cadet, D. Gasparutto, A. Dourandin, N. E. Geacintov, *Chem. Res. Toxicol.* **2001**, *14*, 233–241.
[55] S. Schindler, E. W. Castner, C. Creutz, N. Sutin, *Inorg. Chem.* **1993**, *32*, 4200–4208.
[56] R. E. Huie, L. C. Shoute, P. Neta, *Int. J. Chem. Kinet.* **1991**, *23*, 541–552.
[57] V. Duarte, J. G. Muller, C. J. Burrows, *Nucleic Acids Res.* **1999**, *27*, 496–502.
[58] W. Luo, J. G. Muller, E. M. Rachlin, C. J. Burrows, *Chem. Res. Toxicol.* **2001**, *14*, 927–938.
[59] M. D. Leipold, J. G. Muller, C. J. Burrows, S. S. David, *Biochemistry* **2000**, *39*, 14984–14992.
[60] M. D. Leipold, H. Workman, J. G. Muller, C. J. Burrows, S. S. David, *Biochemistry*, **2003**, *42*, 11373–11381.
[61] P. M. Cullis, M. E. Malone, L. A. Merson-Davies, *J. Am. Chem. Soc.* **1996**, *118*, 2775–2781.
[62] J. Cadet, A. G. Bourdat, C. D'Ham, V. Duarte, D. Gasparutto, A. Romieu, J. L. Ravanat, *Mutat. Res.* **2000**, *462*, 121–128.
[63] D. J. Patel, A. Pardi, K. Itakura, *Science* **1982**, *216*, 581–590.
[64] A. Spassky, D. Angelov, *Biochemistry* **1997**, *36*, 6571–6576.
[65] V. Shafirovich, A. Dourandin, W. Huang, N. P. Luneva, N. E. Geacintov, *Phys. Chem. Chem. Phys.* **2000**, *2*, 4399–4408.
[66] H.-A. Wagenknecht, S. R. Rajski, M. Pascaly, E. D. A. Stemp, J. K. Barton, *J. Am. Chem. Soc.* **2001**, *123*, 4400–4407.
[67] F. D. Lewis, J. Liu, X. Zuo, R. T. Hayes, M. R. Wasielewski, *J. Am. Chem. Soc.* **2003**, *125*, 4850–4861.
[68] C. J. Burrows, J. G. Muller, *Chem. Rev.* **1998**, *98*, 1109–1151.
[69] V. Shafirovich, A. Dourandin, W. Huang, N. P. Luneva, N. E. Geacintov, *J. Phys. Chem. B* **1999**, *103*, 10924–10933.
[70] W. J. McElroy, *J. Phys. Chem.* **1990**, *94*, 2435–2441.
[71] S. V. Lymar, H. A. Schwarz, G. Czapski, *Radiat. Phys. Chem.* **2000**, *59*, 387–392.
[72] K. L. Ivanov, E. M. Glebov, V. F. Plyusnin, Y. V. Ivanov, V. P. Grivin, N. M. Bazhin, *J. Photochem. Photobiol. A* **2000**, *133*, 99–104.
[73] V. Y. Shafirovich, P. P. Levin, V. A. Kuzmin, T. E. Thorgeirsson, D. S. Kliger, N. E. Geacintov, *J. Am. Chem. Soc.* **1994**, *116*, 63–72.
[74] G. V. Buxton, C. L. Greenstock, W. P. Helman, A. B. Ross, *J. Phys. Chem. Ref. Data* **1988**, *17*, 513–886.
[75] R. Misiaszek, C. Crean, A. Joffe, N. E. Geacintov, V. Shafirovich, *J. Biol. Chem.* **2004**, *279*, 32106–32115.

Received: October 7, 2006
Published online: March 5, 2007

